

B. Babes, N. Hamouda, S. Kahla, H. Amar, S.S.M. Ghoneim

## Fuzzy model based multivariable predictive control design for rapid and efficient speed-sensorless maximum power extraction of renewable wind generators

**Introduction.** A wind energy conversion system needs a maximum power point tracking algorithm. In the literature, several works have interested in the search for a maximum power point wind energy conversion system. Generally, their goals are to optimize the mechanical rotation or the generator torque and the direct current or the duty cycle switchers. The power output of a wind energy conversion system depends on the accuracy of the maximum power tracking controller, as wind speed changes constantly throughout the day. Maximum power point tracking systems that do not require mechanical sensors to measure the wind speed offer several advantages over systems using mechanical sensors. **The novelty.** The proposed work introduces an intelligent maximum power point tracking technique based on a fuzzy model and multivariable predictive controller to extract the maximum energy for a small-scale wind energy conversion system coupled to the electrical network. The suggested algorithm does not need the measurement of the wind velocity or the knowledge of turbine parameters. **Purpose.** Building an intelligent maximum power point tracking algorithm that does not use mechanical sensors to measure the wind speed and extracts the maximum possible power from the wind generator, and is simple and easy to implement. **Methods.** In this control approach, a fuzzy system is mainly utilized to generate the reference DC-current corresponding to the maximum power point based on the changes in the DC-power and the rectified DC-voltage. In contrast, the fuzzy model-based multivariable predictive regulator follows the resultant reference current with minimum steady-state error. The significant issues of the suggested maximum power point tracking method, such as the detailed design process and implementation of the two controllers, have been thoroughly investigated and presented. The considered maximum power point tracking approach has been applied to a wind system driving a 5 kW permanent magnet synchronous generator in variable speed mode through the simulation tests. **Practical value.** A practical implementation has been executed on a 5 kW test bench consisting of a dSPACEs1104 controller board, permanent magnet synchronous generator, and DC-motor drives to confirm the simulation results. Comparative experimental results under varying wind speed have confirmed the achievable significant performance enhancements on the maximum wind energy generation and overall system response by using the suggested control method compared with a traditional proportional integral maximum power point tracking controller. References 24, tables 3, figures 15. **Key words:** small-scale wind generator, maximum power point tracking, fuzzy system, fuzzy model based multivariable predictive control, linear matrix inequalities approach.

**Вступ.** Система перетворення енергії вітру потребує алгоритму відстеження точки максимальної потужності. У літературі є кілька робіт, присвячених пошуку системи перетворення енергії вітру із точкою максимальної потужності. Як правило, їх метою є оптимізація механічного обертання або моменту, що крутить, генератора і перемикачів постійного струму або робочого циклу. Вихідна потужність системи перетворення енергії вітру залежить від точності контролера стеження за максимальною потужністю, оскільки швидкість вітру постійно змінюється протягом дня. Системи стеження за точками з максимальною потужністю, яким не потрібні механічні датчики для вимірювання швидкості вітру, мають ряд переваг у порівнянні з системами, що використовують механічні датчики. **Новизна.** Пропонована робота представляє інтелектуальний метод відстеження точки максимальної потужності, заснований на нечіткій моделі та багатопараметричному прогнозуючому контролері, для отримання максимальної енергії для маломасштабної системи перетворення енергії вітру, підключеної до електричної мережі. Пропонований алгоритм не вимагає вимірювання швидкості вітру або знання параметрів турбіни. **Мета.** Побудова інтелектуального алгоритму відстеження точки максимальної потужності, який не використовує механічні датчики для вимірювання швидкості вітру та витягує максимально можливу потужність з вітрогенератора, а також простий та зручний у реалізації. **Методи.** У цьому підході до управління нечітка система в основному використовується для генерування еталонного постійного струму, що відповідає точці максимальної потужності, на основі змін потужності постійного струму та постійної випрямленої напруги. Навпаки, багатопараметричний прогнозуючий регулятор на основі нечіткої моделі слідує за результируючим еталонним струмом з мінімальною помилкою, що встановилася. Істотні проблеми запропонованого методу відстеження точки максимальної потужності, такі як процес детального проектування та реалізація двох контролерів, були ретельно досліджені та представлені. Розглянутий підхід до відстеження точки максимальної потужності був застосований до вітрової системи, що приводить у дію синхронний генератор з постійними магнітами потужністю 5 кВт у режимі змінної швидкості за допомогою моделювання. **Практична цінність.** Для підтвердження результатів моделювання було виконано практичну реалізацію на випробувальному стенді потужністю 5 кВт, що складається з плати контролера dSPACEs1104, синхронного генератора з постійними магнітами та електроприводів з двигунами постійного струму. Порівняльні експериментальні результати при різній швидкості вітру підтвердили значні поліпшення продуктивності з максимального вироблення енергії вітру і загального відгуку системи при використанні запропонованого методу управління в порівнянні з традиційним пропорційно-інтегральним контролером спостереження за точкою максимальної потужності. Бібл. 24, табл. 3, рис. 15. **Ключові слова:** малогабаритний вітрогенератор, відстеження точки максимальної потужності, нечітка система, багатопараметричне прогностичне управління на основі нечіткої моделі, метод лінійних матричних нерівностей.

**Introduction.** Over the past decades, wind power has grown faster than any other source of renewable energy, national policymakers' concerns about global warming, energy diversification, safety supplies, and other factors have contributed to this enormous growth. Various types of converter topologies have been introduced to generate electricity from wind generators and manage distributed energy towards electrical

networks. Each of them requires a suitable type of generator (e.g., permanent magnet synchronous generators (PMSGs), induction generators (IGs), doubly fed induction generators (DFIGs) [1, 2]. Permanent magnet synchronous wind generators with a six diodes bridge rectifier, followed by a DC-DC boost chopper and a grid inverter seem to be a very good solution for small-

© B. Babes, N. Hamouda, S. Kahla, H. Amar, S.S.M. Ghoneim

scale wind turbines to achieve low cost and complexity, high reliability, and good performance by controlling the electromechanical energy conversion with minimal influence on the electrical network [3, 4], notably if the converter control is exploited with the appropriate maximum power point tracking (MPPT) algorithm. As for the MPPT algorithms, there are many MPPT approaches have been mentioned in the literature.

In most cases, these approaches rely on wind velocity measurement or wind speed-sensorless method, such as duty cycle control method, look-up table for optimum rotor speed control method, and optimum tip-speed ratio (TSR) control method. However, these schemes require precise knowledge of the wind power system parameters either before or during execution.

Moreover, the wind turbine components tend to modify their characteristics over time. Therefore, a control strategy independent of the wind generator parameters does not necessitate any prior information of the wind speed, such as the perturbation and observation (P&O) method, which is very flexible and accurate [5-7]. Moreover, this strategy is straightforward, simple, and suitable for wind generators with low inertia. Recently, there have been many articles on the MPPT methodology, especially the simplified and advanced P&O methods [8], adaptive MPPT method [9], two-stage MPPT algorithm [10], hill-climb searching algorithm [11], and modifiable step size-based P&O algorithm [12]. Despite being simple and adaptable, these MPPT techniques suffer from the problems of high steady-state errors and huge frequency variations. Other MPPT algorithms, such as fuzzy reasoning-based MPPT technique [13], neural network technique [14], and advanced vector technique [15], have also been proposed in the literature. Nevertheless, these

control strategies necessitate extensive calculations and are not always effective. Moreover, these control techniques need extra control efforts as well as costly sensors [16].

**The goal of the paper** is to introduce a new intelligent maximum power point tracking method for a small-scale wind generator connected to the electrical network.

The suggested MPPT technique is mainly based on a fuzzy system for deriving the reference DC-current. An innovative fuzzy model-based multivariable predictive algorithm is used to follow the reference DC-current accurately and then implement the intelligent MPPT algorithm. The suggested MPPT method can capture the maximum amount of energy from a wind generator while retaining excellent performance and quality.

**Subject of investigations.** This article explains how to properly manage important challenges in the design and implementation of the two regulators. Experimental results demonstrate the significant performance enhancements that can be achieved in the maximum power generation and overall system response using the suggested intelligent MPPT method. The two regulators are simple and easy to operate in modern wind power generators equipped with a six diode rectifier and boost circuit.

**System description.** The synoptic schematic of the considered wind power system is illustrated in Fig. 1. The conversion circuit comprises of a wind turbine with three blades, a multi-pole three-phase PMSG, a six-diode bridge rectifier, a DC-DC boost chopper, and a source voltage inverter (VSI), which is coupled to the grid. The harvested wind energy is sent immediately to the PMSG, which is transformed into electrical power by this generator.

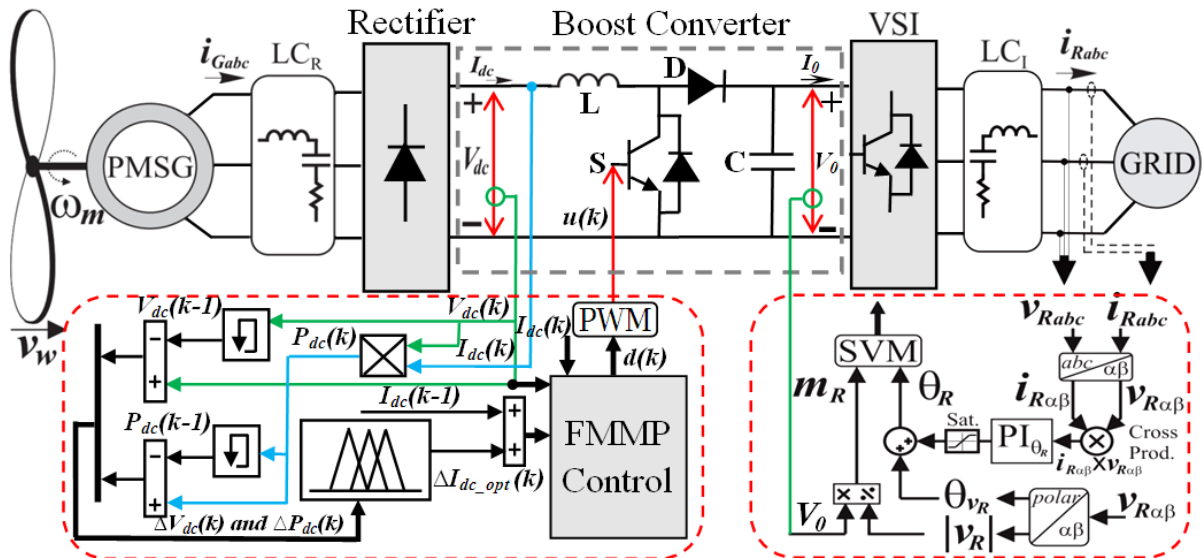


Fig. 1. Synoptic schematic of the considered wind system

The resulting electrical power can then be converted using a conventional rectifier. The boost chopper boosts the rectified DC-voltage ( $V_{dc}$ ), then supplied into the electrical network through the VSI. Because the traditional rectifier is uncontrollable, a boost chopper is employed to guarantee the maximum power capture of electrical energy from the wind generator. Only one

electronic switch is required, which minimizes the system's cost and simplifies its control, consequently maintaining high system reliability and stability [17].

The VSI adjusts the power flow between the DC-bus voltage ( $V_0$ ) and the electrical grid as a result independent grid-side. The mechanical power produced by the wind generator can be expressed as in [18]:

$$P_m = \frac{1}{2} \rho A C_p (\lambda, \beta) v_w^3, \quad (1)$$

where  $\rho$  represents the air mass density;  $C_p$  indicates the performance coefficient of the wind generator;  $A$  denotes the swept surface of the three blades,  $v_w$  denotes the wind velocity;  $\lambda$  is the tip speed ratio (TSR);  $\beta$  is the inclination angle of the blade (in this study set to zero).

A general form is utilized for modeling  $C_p$ . The equation is derived from the characteristics of the wind turbines [19]:

$$C_p = 0.5176 \left( \frac{116}{\lambda_i} - 0.4\beta - 5 \right) e^{-\frac{21}{\lambda_i}} + 0.0068\lambda_i; \quad (2)$$

$$\frac{1}{\lambda_i} = \frac{1}{\lambda + 0.08\beta} - \frac{0.055}{\beta^3 + 1}, \quad (3)$$

where  $\lambda$  is the ratio of the linear turbine rotation to the wind velocity, which is stated as:

$$\lambda = \frac{\omega_m R}{v_w}, \quad (4)$$

where  $\omega_m$  and  $R$  are the turbine rotational speed and radius, respectively.

Figure 2 displays the  $C_p$  against  $\lambda$  graph obtained by (2). It's worth noting, that there is a unique optimum value of the  $\lambda_{opt}$  at which the  $C_p$  is at its highest value  $C_p^{\max}$  [20].

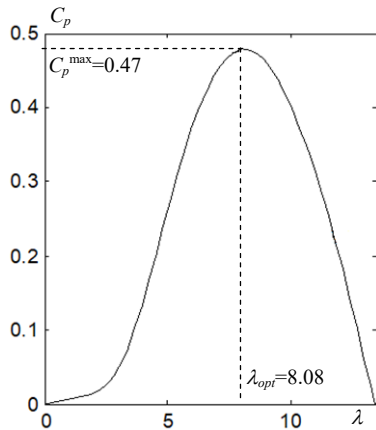


Fig. 2.  $C_p = f(\lambda)$  of the considered wind generator

Thus, the mechanical energy collected from the wind generator is likewise at its peak if the wind generator works at the MPP  $(\lambda_{opt}, C_p^{\max}) = (8.08, 0.47)$ . The optimum mechanical power ( $P_{\max}$ ) can be established by replacing (4) into (1), as shown in:

$$P_{\max} = k_p \omega_{m\_opt}^3, \quad (5)$$

where  $\omega_{m\_opt}$  represents the optimum mechanical angular speed of the wind generator for a given wind velocity;  $k_p$  is the power control coefficient calculated as follows:

$$k_p = \frac{\rho \pi R^5 C_p^{\max}}{2 \lambda_{opt}^3}. \quad (6)$$

From (1), (5) the approximate relationship is obtained:

$$P_{\max} \propto v_w^3 \propto \omega_{m\_opt}^3, \quad (7)$$

where symbol  $\propto$  indicates that the relationship is an approximation between the two variables.

The back-EMF of the PMSG is proportional to rotational velocity, and can be calculated as:

$$E = k_e \omega_m, \quad (8)$$

where  $k_e$  is the back-EMF coefficient of the wind generator.

The phase terminal AC voltage  $V_{ac}$  in the root-mean square (RMS) for a three-phase PMSG is defined as:

$$V_{ac} = E - I_{ac}(R_s + j\omega_e L_s), \quad (9)$$

with:

$$\omega_e = p \omega_m, \quad (10)$$

where  $I_{ac}$ ,  $R_s$ ,  $L_s$  are the line-current in RMS, the line-resistor, and the line inductance, respectively;  $\omega_e$  is the electrical angular speed of the PMSG;  $p$  is the number of pole pairs.

Using a six-diode bridge rectifier, the rectified DC-voltage ( $V_{dc}$ ) is related to the phase-voltage of the PMSG, therefore can be calculated as:

$$V_{dc} = \frac{3\sqrt{6}}{\pi} V_{ac}. \quad (11)$$

Assuming no power losses, the electrical DC-power ( $P_{dc}$ ) can be expressed as:

$$P_{dc} = 3V_{ac} I_{ac} = V_{dc} I_{dc}, \quad (12)$$

where  $I_{dc}$  represents the rectified DC-current, which can be determined by replacing (11) in (12):

$$I_{dc} = \frac{\pi}{\sqrt{6}} I_{ac}. \quad (13)$$

Equations (8)–(10) can then be used to get the following equation:

$$\begin{cases} V_{dc} = \frac{3\sqrt{6}}{\pi} \left( k_e - \frac{\sqrt{6}}{6} p L_s I_{ac} \right) \omega_m; \\ V_{dc}^{opt} = \frac{3\sqrt{6}}{\pi} \left( k_e - \frac{\sqrt{6}}{6} p L_s I_{ac} \right) \omega_m^{opt}, \end{cases} \quad (14)$$

where  $V_{dc}^{opt}$  is the optimum rectified DC-voltage at the MPP.

Substituting (5) into (14) gives:

$$V_{dc} \propto \omega_m \text{ and } V_{dc}^{opt} \propto \omega_m^{opt}. \quad (15)$$

From (5), (14) at the MPP, the following relationship is valid:

$$V_{dc} \propto \omega_m \text{ and } P_{\max} \propto (V_{dc}^{opt})^3. \quad (16)$$

Meanwhile, the optimum DC-power can be described as:

$$P_{dc}^{opt} = \eta P_{\max} = V_{dc}^{opt} I_{dc}^{opt}, \quad (17)$$

where  $\eta$  is the conversion coefficient from the PMSG to the DC-side, which is considered constant;  $I_{dc}^{opt}$  is the optimum DC-current or the reference DC-current ( $I_{dc}^*$ ).

Mixing (16), (17) gives:

$$I_{dc}^{opt} \propto (V_{dc}^{opt})^2. \quad (18)$$

Substituting (18) into (17) yields:

$$I_{dc}^{opt} \propto (P_{dc}^{opt})^{\frac{2}{3}}. \quad (19)$$

As indicated in (18), (19),  $I_{dc}^{opt}$  is proportional to the square of  $V_{dc}^{opt}$ , and is directly related to  $P_{dc}^{opt}$ . As a result, when  $I_{dc}$  is kept close to its optimal (reference  $I_{dc}^*$ ) value  $I_{dc}^{opt}$ , the wind generator may produce the maximum amount of electrical power  $P_{dc}^{\max}$ .

**Fuzzy-based MPPT controller for wind power generator.** The main objective of this section is to

construct a MPP current-reference generator by using a fuzzy logic controller that meets the actual MPP. In particular, this generator is designed to compute on-line the optimal DC-current value  $I_{dc}^{opt}$ . So that, if the DC-current  $I_{dc}$  is being equal to  $I_{dc}^{opt}$  then, the maximal power is captured. The key benefit of this MPPT system is that it doesn't necessitate the use of either wind velocity sensors or rotor velocity sensors. Generally, the fuzzy system can be divided into three steps: 1) fuzzification; 2) aggregation, and 3) defuzzification. As shown in Fig. 1, the  $P_{dc}$  and  $V_{dc}$  variations are selected as the two input parameters for the fuzzy MPPT system. At the  $k^{\text{th}}$  sampling period, both variables are calibrated by the scaling gains  $K_1$ ,  $K_2$ , and updated using the following equations:

$$\Delta P_{dc}[k] = K_1(\Delta P_{dc}[k] - \Delta P_{dc}[k-1]); \quad (20)$$

$$\Delta V_{dc}[k] = K_2(\Delta V_{dc}[k] - \Delta V_{dc}[k-1]), \quad (21)$$

where  $\Delta P_{dc}[k]$  and  $\Delta V_{dc}[k]$  are the DC-power and the DC-voltage variations, respectively;  $P_{dc}[k]$ ,  $V_{dc}[k]$ ,  $P_{dc}[k-1]$  and  $V_{dc}[k-1]$  represent the DC-power and the DC-voltage at the time interval  $[k]$  and  $[k-1]$ .

The DC-power can be determined as:

$$P_{dc}[k] = V_{dc}[k] \cdot I_{dc}[k], \quad (22)$$

where  $I_{dc}[k]$  and  $V_{dc}[k]$  are the DC-current and the DC-voltage at the time interval  $k$ .

The change in the optimum DC-current  $\Delta I_{dc}[k]$  is used as an output of the proposed fuzzy MPPT generator. To create the fuzzy sets of inputs and output variables, the triangular symmetrical membership functions (MFs) with the overlap are utilized to make the fuzzy MPPT system more sensitive to small signals, illustrated in Fig. 3.

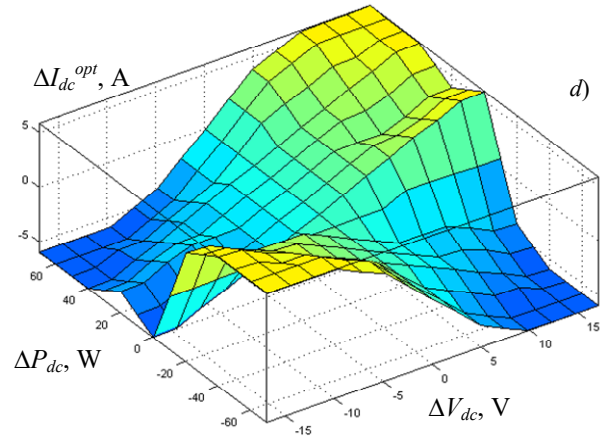
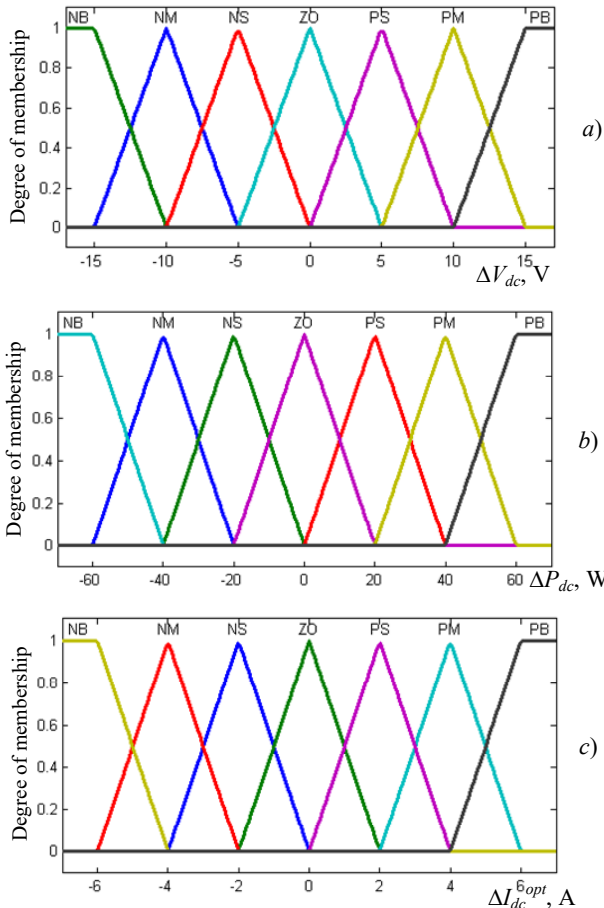


Fig. 3. Normalized membership functions (MFs) and corresponding surface view

The input/output parameters, i.e.  $\Delta P_{dc}[k]$ ,  $\Delta V_{dc}[k]$  and  $\Delta I_{dc}^{opt}[k]$  are represented by linguistic terms, such as Positive-Big (PB), Positive-Medium (PM), Positive-Small (PS), Zero (ZE), Negative-Big (NB), Negative-Medium (NM), and Negative-Small (NS).

The following IF-THEN rules define the desired relationships between inputs and outputs:

$R_i$ : **IF**  $\Delta P_{dc}[k]$  is  $A_i$  and  $\Delta V_{dc}[k]$  is  $B_j$ , **THEN**  $\Delta I_{dc}^{opt}[k]$  is  $C_k$ , where  $i, j = 1, 2, \dots, 7$ ;  $k = 1, 2, 3, \dots, 49$ , where  $A_i$  and  $B_j$  indicate the antecedents and  $C_k$  indicate the consequent parts, respectively.

The IF-THEN rules are summarized in Table 1. This article uses a fuzzy system with Mamdani method for the inference process [21].

Table 1

		Fuzzy control rules						
		$\Delta V_{dc}$						
$\Delta P_{dc}$	$\Delta I_{dc}^{opt}$	NB	NM	NS	ZE	PS	PM	PB
	NB	PB	PB	PB	ZE	NM	NB	NB
	NM	PM	PM	PM	ZE	NS	NM	NM
	NS	PM	PS	PS	ZE	NS	NS	NM
	ZE	NM	NM	NS	ZE	PS	PM	PB
	PS	NM	NS	NS	ZE	PS	PS	PM
	PM	NM	NM	NM	ZE	PS	PM	PM
	PB	NB	NB	NB	ZE	PM	PB	PB

The output level  $\Delta I_{dc}^{opt}[k]$  of each fuzzy rule is normalized by a factor related to the firing strength  $w_i$ , which is calculated from the minimum operation such as:

$$w_i = \min(\mu_{\Delta P_{dc}}(\Delta P_{dc}[k]), \mu_{\Delta V_{dc}}(\Delta V_{dc}[k])), \quad (23)$$

The defuzzification is realized using the centroid method (COA) of a last combined fuzzy set. The last combined fuzzy set is determined by the sum of all rule output fuzzy sets using the maximum aggregation approach [22]. Therefore, the variation in the optimum DC-current  $\Delta I_{dc}^{opt}[k]$  is calculated according to the following relationship:

$$\Delta I_{dc}^{pot}[k] = \frac{\sum_{j=1}^n \mu(\Delta I_{dc}^{opt}(j)) \times (\Delta I_{dc}^{opt}(j))}{\sum_{j=1}^n \mu(\Delta I_{dc}^{opt}(j))}. \quad (24)$$

The output of the fuzzy MPPT system is  $\Delta I_{dc}^{opt}[k]$ , which is converted to the optimum DC-current,  $I_{dc}^{opt}[k]$  by:

$$I_{dc}^{pot}[k] = I_{dc}^{pot}[k-1] + \Delta I_{dc}^{pot}[k]. \quad (25)$$

**Fuzzy model based multivariable predictive (FMMP) regulator.** In this part, a FMMP regulator is developed for a DC-DC boost chopper in order to follow the optimum DC-current ( $I_{dc}^*$ ). The FMMP regulator is effective for DC-DC boost chopper because this control strategy is a sort of control technique that was primarily introduced to regulate constrained linear and nonlinear systems. In addition, the FMMP regulator has a quick dynamic behavior, excellent stability, and robustness against parameter variation in a variety of working conditions.

**Control system design.** Since the PMSG can provide the rectified DC-current ( $I_{dc}$ ), it can be used as a current source. Therefore, only the dynamic of the boost chopper is studied and described in this paper. In the next part, the T-S fuzzy model of the boost chopper is utilized to represent the original nonlinear behavior for the control design goal using the sector nonlinearity method.

**T-S fuzzy model of the DC-DC boost chopper.** As can be seen from Fig. 1, the global nonlinear dynamical behavior of the DC-DC boost chopper in regular state-variable representation can be expressed as follows:

$$\begin{bmatrix} \frac{dI_{dc}}{dt} \\ \frac{dV_o}{dt} \end{bmatrix} = \begin{bmatrix} 0 & -(1-u) \\ -\frac{(1-u)}{C} & -\frac{L}{R_L C} \end{bmatrix} \begin{bmatrix} I_{dc} \\ V_o \end{bmatrix} + \begin{bmatrix} \frac{1}{L} \\ 0 \end{bmatrix} V_{dc}, \quad (26)$$

where  $I_{dc}$  is the input inductor current or DC-current;  $u$  is the equivalent control signal that takes values in the domain  $\{0, 1\}$ ;  $R_L = V_o/I_o$  is the total equivalent resistance;  $V_o$  is the output DC-voltage;  $I_o$  is the output DC-current;  $C$  and  $L$  are the capacitance and inductance values respectively.

Finally, a DC-DC boost chopper's discrete-time state space representation is used to derive (26), considering the sampling period  $T_s$ , and replacing the control signal  $u$  by its respective duty ratio  $D(k)$ . The result of this discretization can be expressed as:

$$\begin{bmatrix} I_{dc}(k+1) \\ V_o(k+1) \end{bmatrix} = \begin{bmatrix} 1 & -\frac{T_s}{L} \\ \frac{T_s}{C} & -\left(\frac{T_s}{R_L C}\right) \end{bmatrix} \begin{bmatrix} I_{dc}(k) \\ V_o(k) \end{bmatrix} + \begin{bmatrix} \frac{(V_{dc}(k) - V_o(k))}{L} \\ -\frac{I_{dc}(k)T_s}{C} \end{bmatrix} D(k). \quad (27)$$

According to the expressions (26), (27) and the T-S fuzzy model [23], the boost chopper can be described by a second-order  $r_i$ -rule fuzzy system. The  $i^{\text{th}}$  rule of the discrete T-S fuzzy model is written as follows:

**Fuzzy rules  $r_i$ :**

**IF**  $w_1(t)$  is  $F_{i1}$  and ... and  $w_g(t)$  is  $F_{ig1}$ , **THEN**  $x(k+1) = A_i x(k) + B_i u(k)$ ; where  $i = 1, 2, \dots, k$ ;  $A_i \in R^{n \times n}$ ,  $B_i \in R^{n \times m}$ ;  $k$  values denote the number of fuzzy rules;  $w_1, w_2, \dots, w_g$  are the premise variables;  $F_{ij}(j = 1, 2, \dots, g)$  are the fuzzy sets;  $x(k) \in R^n$  are the system variables;  $u(k)$  are the control input signal;  $A_i, B_i$  are the state vectors of the local sub-system inadequate sizes.

Using the singleton fuzzification, product inference rule, and weighted average defuzzification, the above fuzzy rules base is deduced as follows:

$$x(k+1) = \sum_{i=1}^k \mu_i(w(k)) \{A_i x(k) + B_i u(k)\}, \quad (28)$$

where:

$$\mu_i(w(k)) = \frac{\prod_{j=1}^g F_{ij}(w_j(k))}{\sum_{i=1}^k \prod_{j=1}^g F_{ij}(w_j(k))}. \quad (29)$$

The term  $F_{ij}(w_j(k))$  is the grad of membership of  $w_j(t)$  in  $F_{ij}$ . Note that, where for  $i = 1, 2, \dots, k$ . For deriving the T-S model of the DC-DC boost chopper, let the fuzzy premises variable vector  $w(k)$  be selected as:

$$w_1(k) = I_{dc}(k), \quad w_2(k) = V_o(k).$$

Since, the system states of the boost chopper are bounded; the premise variables will also be bounded. In this paper, the fuzzy premise variables vary in the range defined as:

$$\max(I_{dc}(k)) = D_1, \quad \min(I_{dc}(k)) = d_1;$$

$$\max(V_o(k)) = D_2, \quad \min(V_o(k)) = d_2.$$

From the above, the corresponding MFs of the T-S system can be written as:

$$F_{11} = \frac{I_{dc}(k) - d_1}{D_1 - d_1}, \quad F_{12} = 1 - F_{11};$$

$$F_{21} = \frac{V_o(k) - d_2}{D_2 - d_2}, \quad F_{22} = 1 - F_{21}.$$

These membership functions are considered triangular shape as demonstrated in Fig. 4.

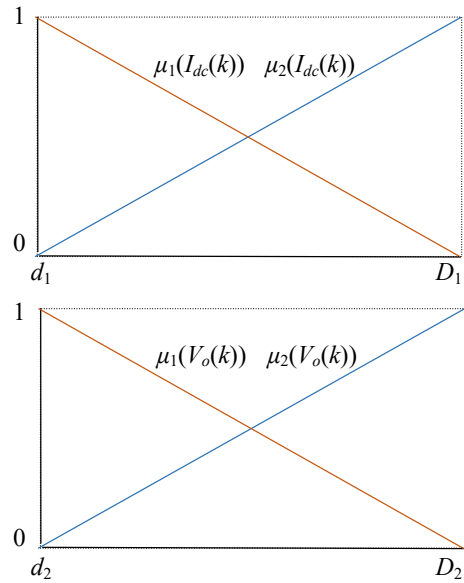


Fig. 4. Picture MFs of the T-S fuzzy model

Based on the sector nonlinearity notion, we have the following relationships:

$$I_{dc}(k) = F_{11}D_1 + F_{21}d_1, \quad V_o(k) = F_{21}D_2 + F_{22}d_2.$$

As a result, the complete fuzzy boost chopper model is equivalent to:

$$x(k+1) = A_i(k) + \left( \sum_{i=1}^4 \mu_i(I_{dc}(k), V_o(k)) B_i \right) d(k), \quad (30)$$

where  $A_i$  and  $B_i$  are the local sub-models matrices given by (for  $i = 1, 2, \dots, 4$ ):

$$A_1 = A_2 = A_3 = A_4 = A = \begin{bmatrix} 1 & -\frac{T_s}{L} \\ \frac{T_s}{C} & 1 - \left(\frac{T_s}{R_L C}\right) \end{bmatrix}$$

and:

$$B_1 = \begin{bmatrix} \frac{(V_{dc} - d_2)T_s}{L} \\ -\frac{d_1 T_s}{C} \end{bmatrix}, B_2 = \begin{bmatrix} \frac{(V_{dc} - d_2)T_s}{L} \\ -\frac{D_1 T_s}{C} \end{bmatrix}$$

It can be seen that (30) corresponds with the system (27) inside the polytope area  $[d_1, D_1] \times [d_2, D_2]$ . This operating space is shown in Fig. 5.

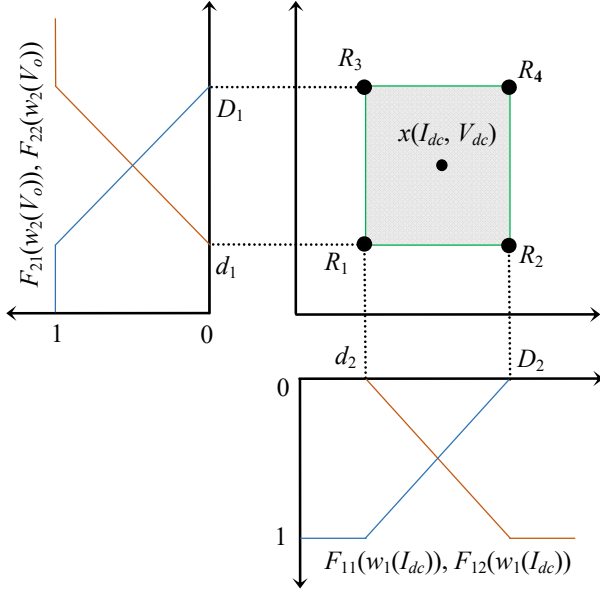


Fig. 5. T-S Fuzzy representation of the boost chopper

**Multivariable predictive current control.** A multivariable predictive current control method based on the T-S fuzzy model is introduced to obtain an accurate tracking control of the optimum DC-current ( $I_{dc}^{opt}$ ) for the DC-DC boost chopper. In this work, the boost chopper's state variables are restricted by physical limits required by the wind generator users due to the technical specifications of the power converters. Therefore, constraints must be set while designing the boost chopper regulator. The primary function of the multivariable predictive control (MPC) is to compute a series of future operating signals in such a way that it reduces a specified objective function calculated over a prediction horizon [24]. The quadratic objective function to be minimized by the MPC controller is given by:

$$\min J = \sum_{j=H_w}^{H_p} (r(k+j) - \hat{y}(k+j|k))^T Q (r(k+j) - \hat{y}(k+j|k)) + \sum_{j=1}^{H_u} (u(k+j-1))^T \Delta u(k+j-1)^T S \Delta u(k+j-1) \quad (31)$$

Subject to the following constraints:

$$x_{\min} \leq \hat{x}(k+j|k) \leq x_{\max}; \quad y_{\min} \leq \hat{y}(k+j|k) \leq y_{\max};$$

$$u_{\min} \leq \hat{u}(k+j|k) \leq u_{\max}; \quad \Delta u_{\min} \leq \Delta u(k+j|k) \leq \Delta u_{\max},$$

where  $k$  is the current sampling instant;  $H_u$  indicates the control cost horizon;  $H_w$  denotes the start point of the prediction horizon;  $H_p$  signifies the end point of the prediction horizon;  $H_u < H_p$ , and  $\Delta u(k+j-1)$  represents the control increments vector,  $r(k+j)$  is the future reference trajectory,  $y(k+j|k)$  is the  $j$  step-ahead prediction of the system;  $Q$  is the weighting matrix of the tracking error;  $R$  and  $S$  are the weighting matrices.

Thus, two parts determine the objective function (32): the first part is concerned with reducing the difference between predicted output and reference trajectory. The second part is a penalty for exerting control effort. Further, the above-mentioned objective function can be defined in a more comprehensive matrix form [25]:

$$J(\Delta U_n) = J_{\min} + 2[\Gamma + \Theta \bar{U}_{k-1} - Y_{ref}^n]^T Q \Lambda \Delta U_n + \Delta U_n^T [\Delta^T Q \Lambda + R + S] \Delta U_n, \quad (32)$$

where

$$J_{\min} = Y_{ref}^T Q Y_{ref} + \Gamma^T Q \Gamma - 2Y_{ref}^T Q \Gamma + \bar{U}_{k-1}^T S \bar{U}_{k-1} + \bar{U}_{k-1}^T R \bar{U}_{k-1}, \quad (33)$$

where  $J_{\min}$  represents the minimal cost due to the reference and the unconstrained output response.

The fuzzy model (30) is utilized to predict the output of the system, subject to amplitude and rate saturation on the system states and control inputs:

$$\begin{bmatrix} I \\ -I \\ L \\ -L \\ \Lambda \\ -\Lambda \end{bmatrix} \Delta U_n \leq \begin{bmatrix} \tilde{U}_{\max} \\ -\tilde{U}_{\min} \\ U_{\max} \\ -U_{\min} \\ Y_{\max} - \Gamma \\ -Y_{\max} + \Gamma \end{bmatrix} \quad (34)$$

and

$$I = \begin{bmatrix} 1 & 0 & \dots & 0 \\ 0 & 1 & \dots & 0 \\ \vdots & \vdots & \ddots & \vdots \\ 0 & 0 & \dots & 1 \end{bmatrix} \in R^{H_u+1 \times H_u+1};$$

$$L = \begin{bmatrix} 1 & 0 & \dots & 0 \\ 1 & 1 & \dots & 0 \\ \vdots & \vdots & \ddots & \vdots \\ 1 & 1 & \dots & 1 \end{bmatrix} \in R^{H_u+1 \times H_u+1},$$

where the predicted output may be written as:

$$\hat{Y} = \Gamma + \Lambda \Delta U_n \quad (35)$$

where  $Y \in R^{H_{pn0}}$ ,  $\Gamma \in R^{H_{pn0}}$ ,  $\Lambda \in R^{H_{pn0} \times H_{pni}}$ , and  $\Delta U_n \in R^{H_{pni}}$ ,  $n_0$  and  $n_i$  are the total number of system outputs and inputs;  $\Gamma$  is the unconstrained output response;  $\Lambda \Delta U_n$  is the constrained output response.

So, the new constrained optimization problem minimizes a convex objective function (33), on a convex set (35). This convex objective function has global minima only if the Hessian matrix of the objective function is positive-definite [26]. In the light of the above description, equation (35) can be transformed into the form:

$$\min \Delta U_n(k)^T H \Delta U_n(k) - P^T \Delta U_n(k). \quad (36)$$

The Hessian matrix  $H$  is positive-definite if it satisfies the following condition:

$$\text{rank}(\Lambda) = H_u. \quad (37)$$

Thus, the restrictions (34) can be expressed in one form that can be simply exploited later by the proposed optimization method:

$$\Lambda U_n(k) \leq B. \quad (38)$$

The Schur complement theorem is utilized to make the non-linear criterion (36) in Linear Matrix Inequalities (LMI)

format. Moreover, this theorem can minimize the linear objective function with LMI restrictions [27]. Therefore, the LMI-based problem of central importance to this paper is that of minimizing a linear subject to LMI constraints:

$$\begin{aligned} & \text{minimize } c^T x; \\ & \text{subject to: } F(x) > 0, \end{aligned}$$

where  $F(x)$  is the symmetric matrix that depends affinely on the variable  $x$ , and  $c$  is the real vector. The solution then minimizes the linear term  $c^T x$  [28].

**LMI problem.** An optimization LMI problem necessitates restructuring the main problem to include a linear objective function and strict inequality constraints. Generally, the minimization of a convex quadratic objective  $J(\Delta U_n)$  can be achieved by the following equivalent minimization algorithm:

$$\begin{aligned} & \text{Minimize } \gamma \text{ and finding an acceptable } \Delta U_n \text{ that} \\ & \text{satisfies the following condition:} \\ & J(\Delta U_n) < \gamma. \end{aligned} \quad (39)$$

The relationship (32) can be converted to LMI form using Schur complement [27].

Given:  $Q(x) = Q(x)^T$ ,  $R(x) = R(x)^T$ , and  $S(x)$  depend affinely on  $x$ . Then LMI (41) is equivalent to the inequalities (39):

$$1) \begin{bmatrix} Q(x) & S(x) \\ S(x)^T & R(x) \end{bmatrix} < 0; \quad (40)$$

$$2) \begin{cases} R(x) < 0; \\ Q(x) - S(x)R(x)^{-1}S(x)^T < 0. \end{cases} \quad (41)$$

Although the inequality (39) is strict but not in linear form. Thus, it must be converted by Schur complement theorem into LMI conditions:

$$\begin{aligned} & \min \gamma \in \mathbb{R}^+ \\ & \text{subject to} \end{aligned} \quad (42)$$

$$\begin{bmatrix} 2[\Gamma + \Theta \bar{U}_{k-1} - Y_{ref}^n]^T Q \Lambda \Delta U_n + J_{\min} - \gamma & \Delta U_n^T \\ \Delta U_n & -[\Lambda^T Q \Lambda + R + S]^{-1} \end{bmatrix} < 0.$$

The aforementioned constraints (34) must be written in a diagonal form defining thus a convex matrix space and symmetric. Hence, the final form of the original optimization problem can be presented as LMI terms. Therefore, the objective function can be reformulated as follows:

$$\begin{aligned} & \min \gamma \in \mathbb{R}^+ \\ & \text{subject to:} \end{aligned} \quad (43)$$

$$\begin{bmatrix} 2[\Gamma + \Theta \bar{U}_{k-1} - Y_{ref}^n]^T Q \Lambda \Delta U_n + J_{\min} - \gamma & \Delta U_n^T \\ \Delta U_n & -[\Lambda^T Q \Lambda + R + S]^{-1} \end{bmatrix} < 0.$$

$$\begin{bmatrix} I \\ -I \\ L \\ -L \\ \Lambda \\ -\Lambda \end{bmatrix} \Delta U_n \leq \begin{bmatrix} \tilde{U}_{\max} \\ -\tilde{U}_{\min} \\ U_{\max} \\ -U_{\min} \\ Y_{\max} - \Gamma \\ -Y_{\max} + \Gamma \end{bmatrix}; \quad (44)$$

$$\text{diag}(I \Delta U_n - U_{\max}) \leq 0;$$

$$\text{diag}(-I \Delta U_n + \tilde{U}_{\min}) \leq 0;$$

$$\text{diag}(L \Delta U_n - \tilde{U}_{\max}) \leq 0;$$

$$\text{diag}(-L \Delta U_n + \tilde{U}_{\min}) \leq 0;$$

$$\text{diag}(\Lambda \Delta U_n - Y_{\max} + \Gamma) \leq 0;$$

$$\text{diag}(\Lambda \Delta U_n + Y_{\min} - \Gamma) \leq 0.$$

**Simulation and experimental verifications.** At first, the performance of the suggested control method incorporating fuzzy based MPPT algorithm is thoroughly examined in simulation using MATLAB/Simulink software. Then experimental tests are performed in laboratory to validate the proposed control strategy.

**Simulation investigation of wind energy conversion system (WECS) control system based FMMP current controller.** This part shows the advantages of implementing the derived predictive algorithm and the fuzzy MPPT control scheme. First, the off-line calculations which are necessary for the calculation of the control signal are stated. Second, the system is simulated based on the small-sized wind turbine model, the key parameters utilized in numerical simulations are listed in Table 2. Finally, simulation results that demonstrate the prevalence of the suggested control algorithm are presented. The control problem is to keep the wind generator at the maximum output power while controlling the DC-current of the boost chopper without oscillations, since these oscillations can cause a variety of issues for consumers for example, and the power outage. The discrete time T-S fuzzy system (30) of the boost chopper can be created using a sampling interval of 0.001 ms, the FMMP scheme is developed with the following conditions: the control horizon is  $H_u = 2$ , and the prediction horizon is  $H_p = 20$ . The limitations are selected as:

$$0 \leq I_{dc} \leq 10 \text{ A} \quad \text{and} \quad 0 \leq V_o \leq 600 \text{ V}.$$

An additional restriction on the boost duty cycle is imposed as follow:

$$0 \leq d(k) \leq 0.98.$$

The values of the weighting matrices in (31) are:

$$Q = \text{eye}(H_p),$$

$$S = 0.5 \cdot \text{eye}((H_u + 1)n_i), \quad R = 0.1 \cdot \text{eye}((H_u + 1)n_i).$$

where  $\text{eye}$  returns an  $(n \times m)$  matrix with ones on the main diagonal and zeros elsewhere.

Table 2

System parameters	
Parameters of the PMSG utilized in simulation	Values
Nominal power	5 kW
Nominal voltage	380 V
Pole pairs	4
Nominal torque	9.5 N·m
Nominal speed	3000 rpm
Nominal current	8 A
Back-EMF coefficient	150 V/K·rpm
Stator resistor	0.245 $\Omega$
$d$ -axis inductor	5 mH
$q$ -axis inductor	5 mH
Inertia	5 kg·m <sup>2</sup>

**Simulation results.** The simulation plots of each state variable are shown in Fig. 6,a-h. The outcomes were obtained based on a 50 s variable wind profile. Figure 6,a shows the wind input used in the computer simulations. The variation in the wind velocity comprises high wind velocity ranges from 11 to 13 m/s.

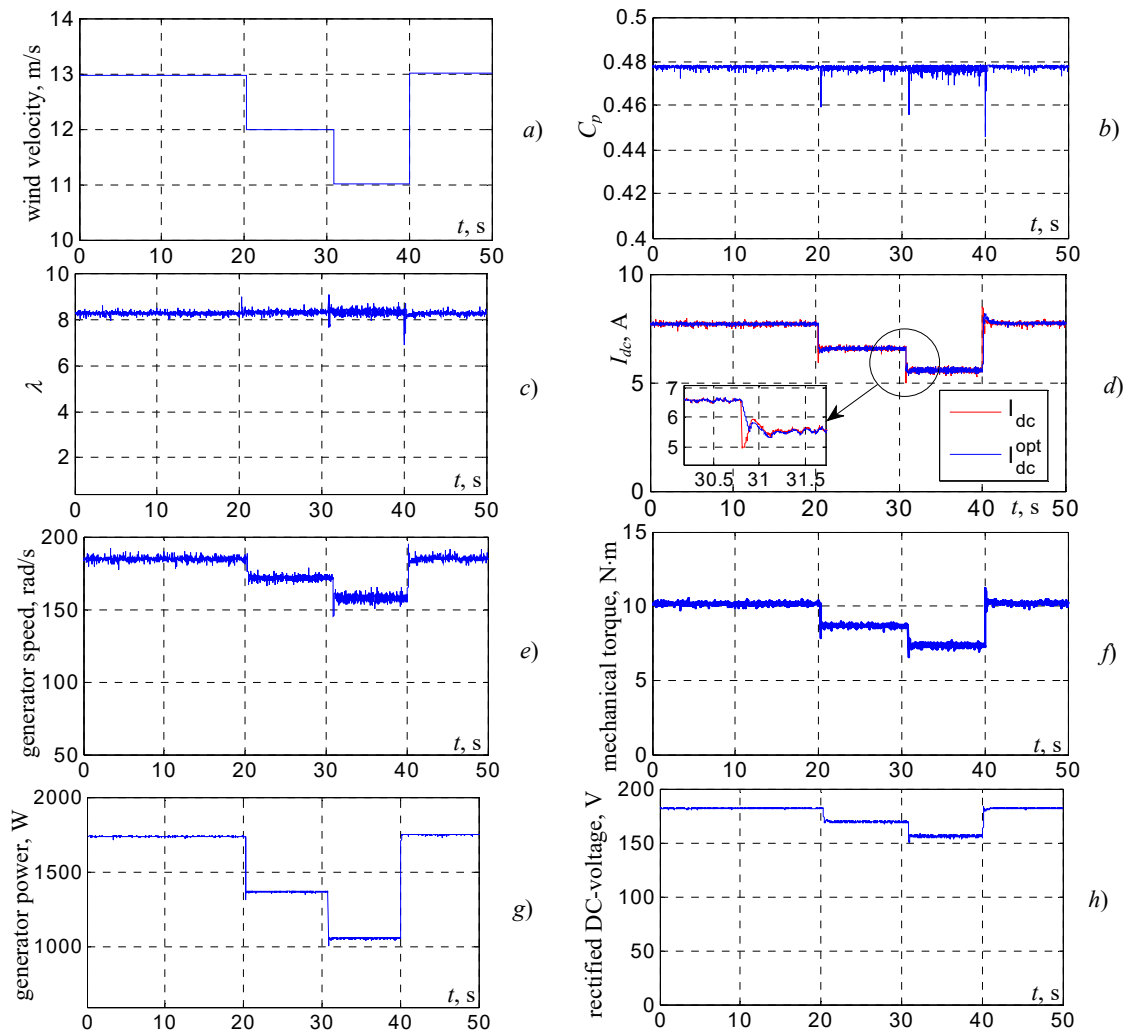


Fig. 6. Simulation results of the fuzzy MPPT algorithm

Figure 6,*b* exhibits the simulated waveform of the  $C_p$ , which is maintained at the optimum value of 0.478, and it is not influenced by the variations in the wind speed, which shows the good performances of the developed fuzzy based MPPT scheme. The resulting TSR is shown in Fig. 6,*c*. It shows that the TSR of the blade remains approximately constant and changes only at limited values around the best TSR of 8.08. It can be observed from Fig. 6,*d*, that the DC-current tracks the optimum current accurately by using the suggested control method, which adjusts the torque generator to obtain the maximum electrical power from the wind turbine with a fast response time. As depicted in Fig. 6,*e*, the rotational speed of the generator is constantly adapted to the wind velocity, so that the maximum energy is captured from the wind generator.

The mechanical torque waveform is illustrated in Fig. 6,*f*, as can be observed from Fig. 6,*f* the torque generator changes according to the variation in wind velocity to accommodate the variations in the DC-current of the boost chopper. Figure 6,*g* displays the generator output power, which is well correlated to changes in wind speed. It can also be noted that using the recommended control technique, the generator output power quickly recovers to its maximum value according to changes in wind velocity. The DC-DC boost chopper can also be used to increase the rectified DC-voltage.

As shown in Fig. 6,*h*, the optimal DC-current is proportional to the rectified DC-voltage, their relationship is in line with (14). Therefore, it can be better controlled to obtain the optimal rectified DC-voltage by using the suggested control approach. The simulation results demonstrate that the designed control method can generate the maximum wind power under different wind speeds by adjusting the DC-current of the boost chopper.

**Experimental verification of WECS control system based on FMMP current controller.** The 5 kW semi-controlled WECS scheme is built in laboratory to prove the effectiveness of the suggested MPPT algorithm. In the experimental WECS, the PMSG is attached to the shaft of a 5 kW DC-motor to emulate the dynamic and static behaviors of the real wind generator. A conventional boost chopper is utilized to drive the DC-motor. The design parameters of the developed WECS prototype are summarized in Table 3.

The boost chopper is built with SEMIKRON IGBT modules, and the driver circuit for the IGBTs modules is SEMIKRON SKHI61. The rectified DC-voltage and DC-current are measured using a voltage sensor and a Hall-effect current sensor, respectively. The proposed intelligent MPPT regulator is implemented using a dSPACE DS1104 controller board installed in a host PC computer, the sampling time is set as 20 kHz, and the

switching frequency of the IGBTs is also kept at 20 kHz. A portable power meter and a digital oscilloscope are utilized to record the experimental results.

The schematic circuit of the complete hardware-setup is depicted in Fig. 7, and the experimental elements of the developed WECS prototype are shown in Fig. 8.

Table 3

System parameters			
Parameters of the WECS for experiments			
PMSG parameters	Values	PMSG parameters	Values
Rated power	5 kW	Torque constant	2.39 N·m/A
Rated voltage	380 V	Mechanical time constant	2.3 ms
Pole pairs	4	DC-motor parameters	
Rated torque	22.5 N·m	Rated current	15 A
Rated speed	2000 rpm	Rated voltage	220 V
Rated current	12 A	Grid-connected converter parameters	
Permanent magnet flux	0.39 Wb	DC-bus capacitance	2200 $\mu$ F
Stator resistor	0.65 $\Omega$	Filter inductor	10 mH
d-axis inductor	8 mH	Filter resistor	0.2 $\Omega$
q-axis inductor	8 mH	Grid voltage	220 V

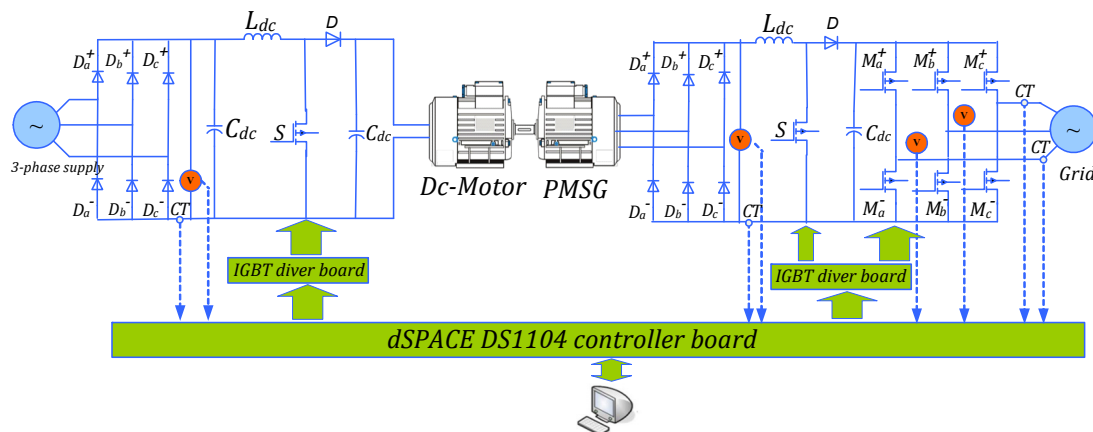


Fig. 7. Arrangement of laboratory system

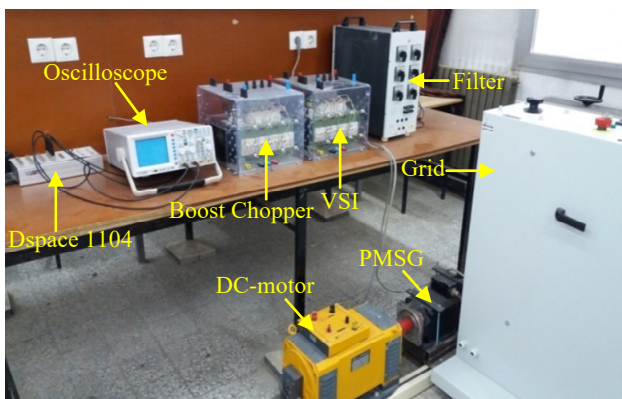


Fig. 8. Laboratory test rig

**Experimental results.** In this part, the performance of the suggested intelligent MPPT algorithm is verified for different wind velocities and compared with that of a traditional PID regulator. In the first test, the wind velocity is step-function or ramp-function changed arbitrarily from 6-8 m/s as illustrated in Fig. 9,a.

The  $C_p$  of the emulated wind turbine and the rectified DC-voltage, the output power of the PMSG (DC-power), and the duty ratio of the boost chopper are illustrated in Fig. 9,b. The obtained results show that a rapid MPP tracking is realized with the proposed intelligent MPPT algorithm.

Despite the change in wind velocity, the real value of  $C_p$  closely matches its optimal value (0.478). Besides

the rapid change in the wind velocity, the rectified DC-voltage and the DC-power are smoothed because of the system inertia.

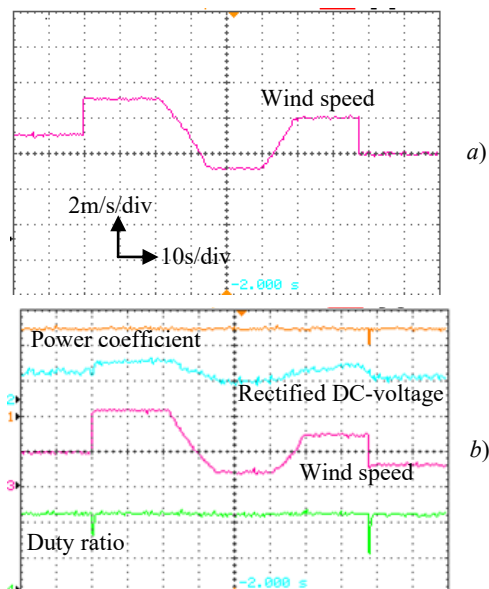


Fig. 9. Experimental results with step-variations in wind velocity

Experiments have also been carried out with time-varying wind speeds. All the waveforms are given in Fig. 10,a,b. It can be observed, that the suggested intelligent MPPT regulator is constantly looking for new MPP.

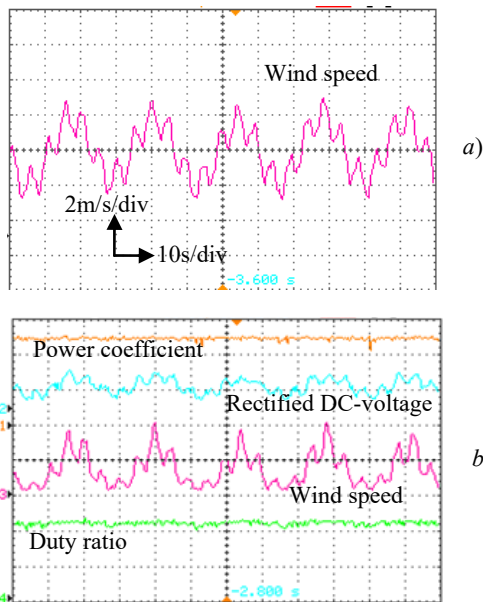


Fig. 10. Experimental results with turbulent wind changes

The functionality of the proposed FMMP current controller was also experimentally verified and compared with the typical PI regulator. The comparison has been done by observing the  $C_p$ , the rectified DC-voltage, the DC-power, and the boost duty cycle waveforms. The test results in Fig. 11 display the programmed switching between the proposed FMMP and PI current control methods. During the last testing scenario, the  $C_p$  and the optimal output power followed their peak values well by utilizing the suggested fuzzy MPPT control method.

The maximum divergence of the  $C_p$  from its peak value is 0.02 with the suggested MPPT method. We can also note that there is no deviation between the real and optimal output powers. On the other hand, when utilizing the traditional PI regulator, the  $C_p$  values oscillate in a larger range, and deviations of electrical power from its peak values are also observed from moment to moment.

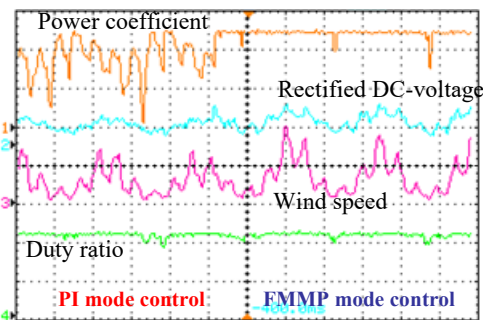


Fig. 11. Comparison of proposed FMMP current controller to conventional PI control method

We can see in Fig. 12, that the electrical energy produced by the wind generator using the suggested intelligent MPPT controller ( $E_{FMMP}$ ) is greater than that produced by the traditional PI control method ( $E_{PI}$ ). Therefore, it proves the effectiveness of the suggested intelligent MPPT controller.

Figure 13 depicts the experimental results of the output three-phase voltage (a) and current (b) of the PMSG for a wind speed of 10 m/s.

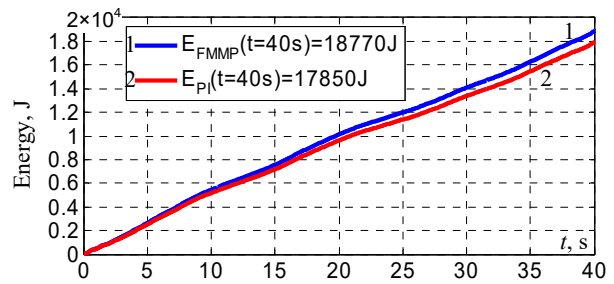


Fig. 12. Total generated electrical energy

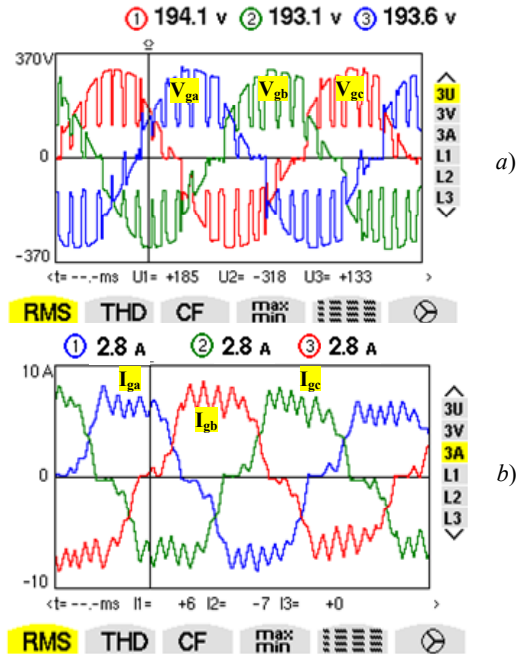


Fig. 13. Experimental waveforms of the WECS with the designed grid-side regulator

Figure 14 illustrates the system performances on the grid-side converter. From Fig. 14,a, it can be seen that all the injected grid currents ( $I_{ga}$ ,  $I_{gb}$ ,  $I_{gc}$ ) and grid voltages ( $V_{ga}$ ,  $V_{gb}$ ,  $V_{gc}$ ) have a sinusoidal shape of 50 Hz. Figure 14,b illustrates Fresnel diagram of the main current and voltage using the classical control of the grid-side converter.

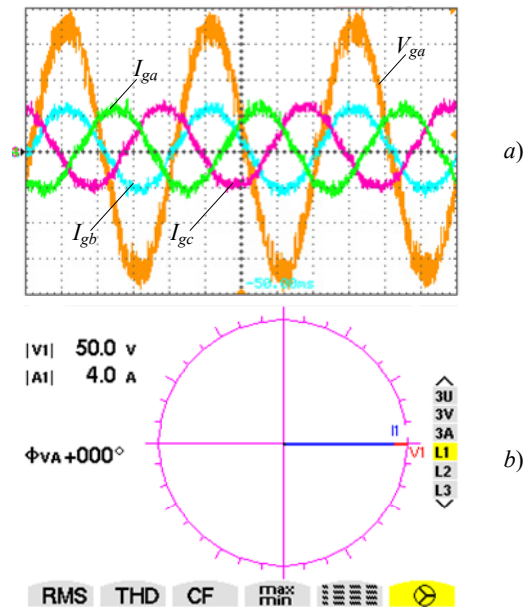


Fig. 14. Experimental results of the WECS with the designed grid-side control algorithm

Finally, Fig. 15,a displays that the total harmonic distortion (THD) of the injected grid current and voltage is 2.5 %, which is below the threshold limit of 5 %. In addition, it meets the requirement of a power factor with a value of 0.996, as depicted in Fig. 15,b.

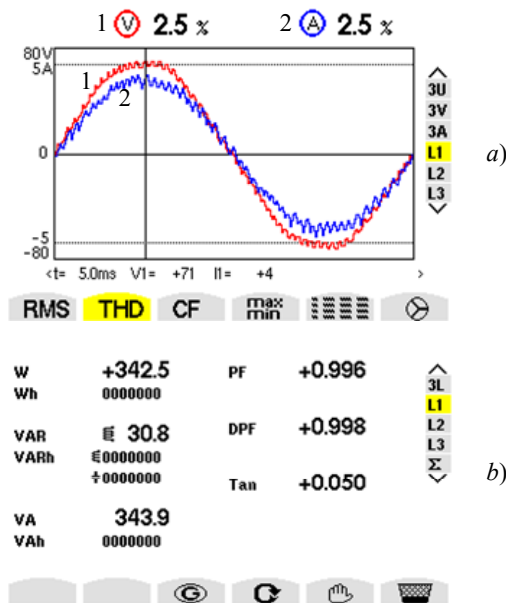


Fig. 15. Experimental results of the WECS with the grid-side control algorithm

### Conclusions.

In this article, an extension of fuzzy model based multivariable predictive current control strategy has been applied to the DC-DC boost chopper of wind energy conversion system to enhance the capability of capturing the maximum output energy based on an intelligent fuzzy maximum power point tracking controller. The considered control algorithm synthesis of the fuzzy model based multivariable predictive controller is based on the fuzzy system, optimization technique, and linear matrix inequalities formulation. In this approach, at every sampling period, a quadratic cost function with a specific prediction horizon and control horizon is minimized such that constraints on the control input are satisfied.

Furthermore, the designed intelligent maximum power point tracking regulator has also been employed to derive the optimum DC-current corresponding to the maximum power point of the wind generator based on the changes in the DC-power and rectified DC-voltage. While the fuzzy model based multivariable predictive current regulator has been designed to follow the derived optimum DC-current with minimum steady-state tracking error, this allows the wind generator to produce the maximum electrical energy.

Simulation and experimental results have affirmed the significant improvements in maximum electrical energy harvesting and mechanical stresses minimization. In addition, compared to the traditional proportional integral controller, the suggested control approach has greater overall control efficiency and can be utilized to harvest maximum wind power more efficiently.

**Conflict of interest.** The authors declare that they have no conflicts of interest.

**Acknowledgment.** The authors express their gratitude to Taif University Researchers Supporting Project Number TURSP-2020/34), Taif, Saudi Arabia.

### REFERENCES

- Babes B., Rahmani L., Chaoui A., Hamouda N. Design and Experimental Validation of a Digital Predictive Controller for Variable-Speed Wind Turbine Systems. *Journal of Power Electronics*, 2017, vol. 17, no. 1, pp. 232-241. doi: <https://doi.org/10.6113/JPE.2017.17.1.232>.
- Amrane F., Chaiba A., Francois B., Babes B. Experimental design of stand-alone field oriented control for WECS in variable speed DFIG-based on hysteresis current controller. *2017 15th International Conference on Electrical Machines, Drives and Power Systems (ELMA)*, 2017, pp. 304-308. doi: <https://doi.org/10.1109/ELMA.2017.7955453>.
- Lee J., Kim Y. Sensorless fuzzy-logic-based maximum power point tracking control for a small-scale wind power generation systems with a switched-mode rectifier. *IET Renewable Power Generation*, 2016, vol. 10, no. 2, pp. 194-202. doi: <https://doi.org/10.1049/iet-rpg.2015.0250>.
- Hamouda N., Babes B., Kahla S., Soufi Y. Real time implementation of grid connected wind energy systems: predictive current controller. *2019 1st International Conference on Sustainable Renewable Energy Systems and Applications (ICSRESA)*, 2019, pp. 1-6. doi: <https://doi.org/10.1109/ICSRESA49121.2019.9182526>.
- Kesraoui M., Korichi N., Belkadi A. Maximum power point tracker of wind energy conversion system. *Renewable Energy*, 2011, vol. 36, no. 10, pp. 2655-2662. doi: <https://doi.org/10.1016/j.renene.2010.04.028>.
- Zhu Y., Cheng M., Hua W., Wang W. A novel maximum power point tracking control for permanent magnet direct drive wind energy conversion systems. *Energies*, 2012, vol. 5, no. 5, pp. 1398-1412. doi: <https://doi.org/10.3390/en5051398>.
- Kazmi S.M.R., Goto H., Guo H., Ichinokura O. A Novel Algorithm for Fast and Efficient Speed-Sensorless Maximum Power Point Tracking in Wind Energy Conversion Systems. *IEEE Transactions on Industrial Electronics*, 2011, vol. 58, no. 1, pp. 29-36. doi: <https://doi.org/10.1109/TIE.2010.2044732>.
- Xia Y., Ahmed K.H., Williams B.W. A New Maximum Power Point Tracking Technique for Permanent Magnet Synchronous Generator Based Wind Energy Conversion System. *IEEE Transactions on Power Electronics*, 2011, vol. 26, no. 12, pp. 3609-3620. doi: <https://doi.org/10.1109/TPEL.2011.2162251>.
- Ching-Tsai Pan, Yu-Ling Juan. A Novel Sensorless MPPT Controller for a High-Efficiency Microscale Wind Power Generation System. *IEEE Transactions on Energy Conversion*, 2010, vol. 25, no. 1, pp. 207-216. doi: <https://doi.org/10.1109/TEC.2009.2032604>.
- Agarwal V., Aggarwal R.K., Patidar P., Patki C. A Novel Scheme for Rapid Tracking of Maximum Power Point in Wind Energy Generation Systems. *IEEE Transactions on Energy Conversion*, 2010, vol. 25, no. 1, pp. 228-236. doi: <https://doi.org/10.1109/TEC.2009.2032613>.
- Lin W.-M., Hong C.-M. Intelligent approach to maximum power point tracking control strategy for variable-speed wind turbine generation system. *Energy*, 2010, vol. 35, no. 6, pp. 2440-2447. doi: <https://doi.org/10.1016/j.energy.2010.02.033>.
- Kazmi S.M.R., Goto H., Guo H.-J., Ichinokura O. A Novel Algorithm for Fast and Efficient Speed-Sensorless Maximum Power Point Tracking in Wind Energy Conversion Systems. *IEEE Transactions on Industrial Electronics*, 2011, vol. 58, no. 1, pp. 29-36. doi: <https://doi.org/10.1109/TIE.2010.2044732>.
- Galdi V., Piccolo A., Siano P. Designing an Adaptive Fuzzy Controller for Maximum Wind Energy Extraction. *IEEE Transactions on Energy Conversion*, 2008, vol. 23, no. 2, pp. 559-569. doi: <https://doi.org/10.1109/TEC.2007.914164>.

14. Pucci M., Cirrincione M. Neural MPPT Control of Wind Generators With Induction Machines Without Speed Sensors. *IEEE Transactions on Industrial Electronics*, 2011, vol. 58, no. 1, pp. 37-47. doi: <https://doi.org/10.1109/TIE.2010.2043043>.
15. Cardenas R., Pena R. Sensorless Vector Control of Induction Machines for Variable-Speed Wind Energy Applications. *IEEE Transactions on Energy Conversion*, 2004, vol. 19, no. 1, pp. 196-205. doi: <https://doi.org/10.1109/TEC.2003.821863>.
16. Chedid R., Mrad F., Basma M. Intelligent control of a class of wind energy conversion systems. *IEEE Transactions on Energy Conversion*, 1999, vol. 14, no. 4, pp. 1597-1604. doi: <https://doi.org/10.1109/60.815111>.
17. Chiang H., Tsai H. Design and implementation of a grid-tied wind power micro-inverter. *IET Renewable Power Generation*, 2013, vol. 7, no. 5, pp. 493-503. doi: <https://doi.org/10.1049/iet-rpg.2012.0342>.
18. Hamouda N., Benalla H., Hemsas K., Babes B., Petzoldt J., Ellinger T., Hamouda C. Type-2 Fuzzy Logic Predictive Control of a Grid Connected Wind Power Systems with Integrated Active Power Filter Capabilities. *Journal of Power Electronics*, 2017, vol. 17, no. 6, pp. 1587-1599. doi: <https://doi.org/10.6113/JPE.2017.17.6.1587>.
19. Beddar A., Bouzekri H., Babes B., Afghoul H. Real time implementation of improved fractional order proportional-integral controller for grid connected wind energy conversion system. *Revue Roumaine Des Sciences Techniques Serie Electrotechnique et Energetique*, 2016, vol. 61, no. 4, pp. 402-407. Available at: [http://revue.elth.pub.ro/upload/89285817\\_ABeddar\\_RRST\\_4\\_2\\_016\\_pp\\_402-407.pdf](http://revue.elth.pub.ro/upload/89285817_ABeddar_RRST_4_2_016_pp_402-407.pdf) (Accessed 12 June March 2021).
20. Kahla S., Bechouat M., Amieur T., Sedraoui M., Babes B., Hamouda N. Maximum power extraction framework using robust fractional-order feedback linearization control and GM-CPSO for PMSG-based WECS. *Wind Engineering*, 2021, vol. 45, no. 4, pp. 1040-1054. doi: <https://doi.org/10.1177/0309524X20948263>.
21. Bose B.K. Expert system, fuzzy logic, and neural network applications in power electronics and motion control. *Proceedings of the IEEE*, 1994, vol. 82, no. 8, pp. 1303-1323. doi: <https://doi.org/10.1109/5.301690>.
22. Mamdani E.H., Assilian S. An Experiment in Linguistic Synthesis with a Fuzzy Logic Controller. *International Journal of Human-Computer Studies*, 1999, vol. 51, no. 2, pp. 135-147. doi: <https://doi.org/10.1006/ijhc.1973.0303>.
23. Takagi T., Sugeno M. Fuzzy identification of systems and its applications to modeling and control. *IEEE Transactions on Systems, Man, and Cybernetics*, 1985, vol. SMC-15, no. 1, pp. 116-132. doi: <https://doi.org/10.1109/TSMC.1985.6313399>.
24. Wang L. *Model predictive control system design and implementation using MATLAB*. Springer London, 2009. doi: <https://doi.org/10.1007/978-1-84882-331-0>.

Received 08.02.2022

Accepted 23.03.2022

Published 01.06.2022

Badreddine Babes<sup>1</sup>, Senior Researcher A,  
 Nouredine Hamouda<sup>1</sup>, Senior Researcher A,  
 Sami Kahla<sup>1</sup>, Senior Researcher A,  
 Hichem Amar<sup>1</sup>, Senior Researcher B,  
 Sherif S.M. Ghoneim<sup>2</sup>, PhD, Associate Professor,  
<sup>1</sup>Research Center in Industrial Technologies CRTI,  
 P.O. Box 64, Cheraga 16014 Algiers, Algeria,  
 e-mail: elect\_babes@yahoo.fr (Corresponding author),  
 n.hamouda@crti.dz, s.kahla@crti.dz, h.amar@crti.dz,  
<sup>2</sup>Department of Electrical Engineering,  
 College of Engineering, Taif University,  
 Taif 21944, Saudi Arabia,  
 e-mail: s.ghoneim@tu.edu.sa

How to cite this article:

Babes B., Hamouda N., Kahla S., Amar H., Ghoneim S.S.M. Fuzzy model based multivariable predictive control design for rapid and efficient speed-sensorless maximum power extraction of renewable wind generators. *Electrical Engineering & Electromechanics*, 2022, no. 3, pp. 51-62. doi: <https://doi.org/10.20998/2074-272X.2022.3.08>